NUMERICAL ANALYSIS OF THE INTERFERENCE EFFECTS ON RESISTANCE, SINKAGE AND TRIM OF A FAST CATAMARAN

Wei He[1,3], Teresa Castiglione[2], Manivannan Kandasamy[1] and Frederick Stern[1]

1 IIHR- Hydroscience and Engineering, The University of Iowa, Iowa City, Iowa, USA
2 Department of Mechanical Engineering, University of Calabria, Arcavacata di Rende, Cosenza, Italy
3 School of Naval Architecture, Ocean and Civil Engineering, Shanghai Jiao Tong University, Shanghai, China

[1,2] gave equal contribution to the present work

Corresponding author: frederick-stern@uiowa.edu

ABSTRACT

The purpose of the present paper is the numerical investigation of the interference phenomena between the waves generated by the individual hulls of a catamaran. The study focuses on the effects of both Froude number and demi-hull separation distance on resistance and on sinkage and trim. The numerical simulations are carried out by the URANS solver CFDShip-Iowa V.4 and, in order to assess the capability for prediction of resistance, sinkage and trim of the URANS code for twin-hull configuration vessels, a verification and validation study is performed for global as well as for local variables. A very good agreement between the numerical results and the experimental data is obtained and the validation study demonstrates the high level of accuracy of the current predictions, which are used to have a better insight into the interference phenomena. In

accordance with the experiments, within *Fr=0.45-0.65*, the catamaran has a significantly higher resistance coefficient compared to the mono-hull; furthermore, the C_T value increases with decreasing the separation distance between the twin hulls. On the contrary, at *Fr* lower than 0.45 and at *Fr* higher than 0.65, the effects of hull spacing on resistance as well as on sinkage and trim can be neglected. The flow field characteristics, wave pattern, wave cuts and pressure distributions are analyzed through the CFD analysis. Finally, the effects of the Reynolds number on resistance are also investigated and results show a small decrease in interference with increasing the Reynolds number.

KEY WORDS

URANS, Catamaran, Interference, Verification and Validation, CFD, Ship motions, Resistance

LIST OF SYMBOLS

b	beam of the demi-hull [-]
C_f	frictional resistance coefficient [-]
C_p	pressure resistance coefficient [-]
C_r	residuary resistance coefficient [-]
C_T	total resistance coefficient [-]
$C_{T,\,cat}$	catamaran total resistance coefficient [-]
$C_{T,\,mono}$	mono-hull total resistance coefficient [-]
D	experimental data value
E	comparison error

Fr	Froude number $\left(=U/\sqrt{gL_{PP}}\right)$
g	acceleration of gravity (=9.81 m/s^2)
h	water depth [m]
IF	interference coefficient [-]
k	turbulent kinetic energy [J/kg]
L_{PP}	model length [m]
n	normal direction
p	order of accuracy, pressure [N/m^2]
p_{th}	estimated order of accuracy
p_{RE}	Richardson extrapolation order of accuracy
P	estimated order of accuracy $\left(=\frac{p}{p_{th}}\right)$
r	grid refinement ratio
R	ratio between solution changes
Re	Reynolds number $\left(=rUL/n\right)$
R_T	total resistance [N]
$R_{T,cat}$	catamaran total resistance [N]
$R_{T,mono}$	mono-hull total resistance [N]
S	separation distance between the hulls [m], wet surface area [m^2]
S_j	simulation value with grid j
s	non-dimensional separation distance (=S/L_{PP})
T	model draft [m]
(U,V,W)	model velocity components [m/s]
U_D	data uncertainty
U_{FB}	facility bias uncertainty

U_G	grid uncertainty
U_I	iterative uncertainty
U_{SN}	numerical simulations uncertainty
U_V	validation uncertainty
(x,y,z)	absolute earth-fixed coordinates
(X,Y,Z)	non-dimensional coordinates
β	turbulence model constant [-]
δ_{RE}	numerical error computed by Richardson extrapolation
ε	turbulence dissipation rate [J/kgs]
ε_{ij}	difference between solutions *i* and *j*
ϕ	free surface level set function
λ	wave length [m]
ρ	water density [kg/m^3]
σ	non-dimensional sinkage
τ	trim [rad]
ζ_{max}	highest wave elevation [m]
ω	specific turbulence dissipation [1/s]

1. INTRODUCTION

Multi-hull surface ships are attractive for high-speed uses due to their favorable resistance, transversal stability, and load characteristics in comparison to conventional mono-hulls. Hull types and applications vary considerably: from relatively small foil-assisted high-speed ferries to relatively large SWATH high-speed sea-lift vessels designed for military transportation. As a consequence, several studies on multi-hull configurations, and in particular on catamarans, have been carried out both experimentally and numerically over the years.

The experimental tests conducted by Insel and Molland (1992) and Molland (1996), on a high-speed catamaran with symmetric demi-hulls, focus on the effects of hull dimensions and of separation distance, on resistance, sinkage and trim, over a wide range of Froude number values (0.2-1.0). They also developed a numerical model, based on the thin strip hypothesis, in order to investigate the catamaran hydrodynamic characteristics. Cheng *et al.* (2003) developed a mathematical theory for the practical design of an asymmetric demi-hull, the *S*-catamaran, whose hull sections were theoretically determined to eliminate or at least substantially reduce wave resistance at supercritical design speeds in shallow water. Further experimental and theoretical investigation of the interference phenomena was also carried out in Millward (1992) and Molland *et al.* (2004). Souto-Igleasias *et al.* (2007) investigated experimentally the influence of the distance between catamaran hulls on wave resistance. They also measured the wave cuts between the two hulls in order to correlate the shapes of the inner wave cuts with the interference resistance and found the possibility of favorable interference for catamarans.

From a numerical and theoretical point of view, the approaches used for investigation of wave interference effects were commonly based on potential flow theory (Moraes *et al.*, 2004; Tarafder and Suzuki, 2007; Yeung and Wan, 2008; Aubault and Yeung, 2009). Bruzzone and Ferrando (1995) used a boundary element method in order to study hull separation length effects. Despite the mentioned studies being quite useful to estimate the wave-making resistance and ship motions, issues remain for design improvements, regarding multi-hull interference, reduced wake signatures, deep/shallow water maneuvering, potential flow vs. CFD capability, and optimization. So far, only a few studies have introduced CFD methods for the analysis of multi-hull vessels. Stern *et al.* (2006a and 2008), have shown interference induced longitudinal vortices for SWATH. Kandasamy *et al.* (2011a) demonstrated the possibility of reduced wake signatures for foil-assisted catamarans. Milanov *et al.* (2011) discussed about the most

relevant issues for improvement of high-speed catamaran deep/shallow water course stability design and of systems-based method predictions.

Recently, the Delft catamaran (Van't Veer, 1998 a, b) has been selected as an international benchmark for research and CFD validation for the Office of Naval Research Naval International Cooperative Opportunities in Science & Technology Program (NICOP) and NATO Advanced Vehicle Technology projects. Several hydrodynamic topics have been assessed about this geometry, by carrying out both experimental tests and numerical studies. They include calm water resistance and seakeeping assessment (Broglia *et al.*, 2011a,b; Castiglione *et al.*, 2011; Zaghi *et al.*, 2011; Broglia *et al.*, 2012; Bouscasse *et al.*, 2013), interference effects (Castiglione *et al.*, 2013; Broglia *et al.*, 2014), deep/shallow water maneuvering (Milanov *et al.*, 2011; Visonneau *et al.*, 2012), waterjet propelled optimization (Kandasamy *et al.*, 2011b) and stochastic uncertainty quantification and optimization (Chen *et al.*, 2013; Diez *et al.*, 2013a,b). The numerical studies have been carried out by the use of RANS methods; the use of adaptive grid refinements in Visonneau *et al.* (2012) is worth mentioning.

The present study contributes to this research with the main objective to assess current URANS capability for a high-speed catamaran, including sinkage and trim. In particular, the effects of Froude number (Fr) and demi-hull separation distance (s) on resistance, sinkage and trim for the Delft catamaran, are investigated. Simulations are carried out for speed values ranging within $0.3 \leq Fr \leq 0.8$ and include several hull spacing values varying within $0.17 \leq s \leq 0.30$. The methodology used in this work is as follows: a quantitative verification and validation (V&V) study is performed for Fr=0.5 at the design hull separation distance corresponding to s=0.23, using available benchmark validation data. Once the code is validated, the numerical results are used to have a better insight in the flow field characteristics around the twin hulls; in particular wave pattern, wave cuts in the inner region between hulls and pressure distributions along the hull will be analyzed. Finally, a Reynolds number (Re) study is also included in order to

investigate the effects of viscosity on interference.

2. OVERVIEW OF EXPERIMENTAL DATA

The main particulars of the Delft catamaran are provided in Figure 1 and Table 1. For the design separation distance, *s=0.23*, calm water resistance, sinkage and trim experiments were carried out at three facilities: TU Delft (Van't Veer, 1998), BSHC (Zlatev *et al.*, 2009), and INSEAN (Broglia *et al.*, 2014). The experimental uncertainty (U_D) is provided by INSEAN at Fr=0.5, 0.65 and 0.75. Table 1 also includes the facility bias, U_{FB}, which is estimated by comparing the available data, according to the following approach:

$$U_{FB} = \begin{cases} D_{Avg}^{j} = \frac{1}{M}\sum_{i=1}^{M} D_i^j \\ E_i^j = D_i^j - D_{Avg}^j \\ U_{FB,i} = \frac{1}{2}\left[Max\left(\left|E_i^j\right|\right) - Min\left(\left|E_i^j\right|\right)\right] \; j = 1..N \end{cases} \tag{1}$$

where M is the number of facilities where tests are performed, and D_i^j is the observation in i^{th} facility at j^{th} Fr. Facility bias is studied in the Fr range 0.25 - 0.6 for which the data between facilities overlap.

A comparison of EFD data among the three facilities, at the design separation distance *s=0.23*, is shown in Figure 2. It includes total resistance coefficient, C_T, with its friction (C_f) and residuary (C_p) components, and non-dimensional sinkage and trim as functions of the Froude number, Fr. The total resistance coefficient is defined as $C_T=R_T/(0.5\rho U^2 S)$, where R_T is total resistance [N], ρ is density of the water, U is the

undisturbed velocity and S is the hull wetted surface at rest; the non-dimensional sinkage is defined as $\sigma=sinkage/L_{PP}$, and the trim angle is expressed as τ, [rad]. The measurements have similar trends, but fairly large differences between the facilities occur as indicated by the large U_{FB} values, especially for sinkage and trim at high Fr. They are due to the different model lengths, depths of the towing tank, temperature and center of gravity position between facilities. Furthermore, TU Delft and INSEAN use conventional resistance single-point mounts, whereas BSHC uses a Planar Motion Mechanism two-point mount. Finally, turbulence simulators are used for INSEAN and TU Delft models but not for BSHC.

INSEAN also provides resistance, sinkage and trim data for the mono-hull and for the catamaran with five separation distances, which vary within 0.17 and 0.30, and for several speed values (Fr=0.3÷0.8). The experimental data include the interference coefficient (IF), which is defined as the difference between the total resistance coefficients of the catamaran and the mono-hull, $C_{T,cat}$ and $C_{T,mono}$ respectively, divided by the mono-hull total resistance coefficient, according to:

$$IF = \frac{C_{T,cat} - C_{T,mono}}{C_{T,mono}} = \frac{R_{T,cat} - R_{T,mono}}{2R_{T,mono}} \qquad (2)$$

It gives a measure of the interaction between the twin-hulls waves systems. It is common, in fact, that for a wide range of ship speed values, the resistance experienced by the twin-hull is higher than twice that of the mono-hull ($R_{T,cat}=2R_{T,mono}+R_{IF}$). The additional resistance component is due to the interaction between the waves leaving from each demi-hull, which interact in the inner region. In some cases, negative IF values can occur; the waves systems tend to cancel each other out and cause, therefore, a decrease of wave resistance.

For current URANS simulations, the INSEAN-CNR experimental data (Broglia *et al.*,

2014) will be used for validation purpose. It should be noted that the Reynolds number for CFD simulations is slightly different from the experimental value; this is due to the different water temperature values used between the experiments and the numerical simulations (Table 1). In fact, during the experimental activity it is quite complex to maintain the towing tank water temperature accurate at a prescribed value; consequently, the Reynolds number is usually affected by uncertainty due to changes in viscosity. It is then conventional to use a Reynolds number correction of the experimental data in order to match *Re* at 15 °C for consistency, which is the temperature value used for numerical simulations.

3. COMPUTATIONAL AND ANALYSIS METHOD

3.1 Computational method

The code, used for the current simulations, is CFDShip-Iowa V.4 (Carrica *et al.*, 2012). It is based on the solution of the unsteady Reynolds Averaged Navier-Stokes equations for the liquid phase of a free surface flow. The free surface is captured using a single-phase level-set method (Carrica *et al.*, 2007) and the turbulence is modeled by a blended k-ε/k-ω model (Menter, 1994), without wall functions. Numerical methods include advanced iterative solvers and second and higher order finite difference schemes with conservative formulations. Mass conservation is enforced using a PISO algorithm, resulting in a Poisson equation for pressure. CFDShip-Iowa allows the computation of ship motions (6DOF) by the use of a dynamic overset-grid approach for local grid refinement and large-amplitude motions. In this case, the code SUGGAR (Noack, 2005) is used to obtain the overset domain connectivity between the set of overlapping grids. The simulations run on HPC cluster Cray XT4 (Jade).

3.2 Domain, boundary condition, grids and simulation conditions.

The computational domain includes a background orthogonal grid and a boundary-layer curvilinear grid conforming to ship geometry. Some particulars of the computational domain are depicted in Figure 3. Overall, the grid consists of 3 blocks. The background is a Cartesian block, which is clustered near the free surface to resolve the wave field. Its boundaries are $-0.4 \leq X \leq 3.6$, $0 \leq Y \leq 1.3$ and $-0.7 \leq Z \leq 0.7$, where the coordinates X, Y and Z are non-dimensional with the length between perpendiculars, L_{PP}. For each demi-hull, two body-fitted "O" type grids are generated around the hull geometry. Splash and wave breaking were observed in the experiment; therefore, an unsteady solution of the full ship, which allows asymmetric modes, may be more accurate. However, owing to the computational demand for resolving the current flow, a symmetry boundary condition is applied with respect to $Y=0$ and only half of the catamaran is simulated. The ship axis is aligned with the x-axis with the bow at $X=0$ and the stern at $X=1$, as shown in Figure 1. The free surface at rest lies at $Z=0$.

The boundary conditions are summarized in Table 2. They are specified for each face of the computational domain and proper values are set for each flow variable. At Inlet *(X=-0.4)*, the free-surface level set function, which is zero on the free surface, is given by $\phi=-z$; pressure is zero-gradient; turbulence is set to free stream values and the velocity field is set to the free stream velocity vector *(U,V,W)*. At Exit *(X=3.6)*, the boundary is assumed far downstream so that stream-wise viscous effects are zero ($\frac{\partial^2 U}{\partial n^2} = \frac{\partial^2 V}{\partial n^2} = \frac{\partial^2 W}{\partial n^2} = 0$); other variables are zero-gradient due to domain truncation. Two far-field boundary conditions are used to limit the domain along Y and Z axes. Furthermore, $\frac{\partial f}{\partial n} = +1$ at $Z=-0.7$, indicates that the surface is in contact with the liquid phase; $\frac{\partial f}{\partial n} = -1$ at $Z=+0.7$ indicates the contact between the top background surface and air. Finally, on the ship hull a no-slip boundary condition is imposed, in which the value

for ω is suggested by Menter (1994) and is strictly related to the use of the blended κ-ε/κ-ω turbulence model.

Six grids are used for the current studies: the number of grid points range from 0.8M to 38.1M. Grids G1, G2, G3 and G4 are generated with refinement ratio $\sqrt{2}$. They are used for quantitative verification and validation study and enable two grid triplet studies. Grid G2 is also used for interference study, while grid G2a, generated for the study of Reynolds number effects, is obtained by reducing the near wall distance in G2. Finally, for improved wave elevation predictions, a Cartesian refinement block between the demi-hull and symmetry plane is added to G1 to form grid G1R. Table 3 and Table 4 summarize the grids dimensions and the research studies, respectively.

4. RESULTS

This section presents the results of the numerical simulations. Verification and validation study is carried out for integral variables (resistance coefficients, sinkage and trim) as well as for local variables (longitudinal wave cuts); the analysis of the flow field, in terms of wave pattern and wave profiles, with focus on demi-hull separation effects is shown. Finally, the influence of the Reynolds number on interference is investigated.

4.1 Verification and Validation for resistance, sinkage and trim

In order to benchmark current URANS capability for a high-speed catamaran, including sinkage and trim, quantitative verification and validation (V&V) is required. Verification and validation follows the approach presented in Stern et al. (2006b), while for numerical uncertainty, U_{SN}, the factor of safety method proposed by Xing and Stern (2010) is adopted. Quantitative V&V is conducted for $s=0.23$ and Fr=0.5, for resistance (C_T), sinkage and trim.

The verification study is carried out for two grid triplets: (G1, G2, G3) and (G2, G3, G4). The results are summarized in Table 5. *R* is the convergence ratio, defined as:

$$R = \frac{S_2 - S_1}{S_3 - S_2} \tag{3}$$

where S_1, S_2 and S_3 are the integral or local numerical solutions corresponding to the fine, medium and coarse grid, respectively. When monotonic convergence is achieved ($0<R<1$), the generalized Richardson extrapolation is used for estimation of numerical error and uncertainty. Consequently, the Richardson extrapolation numerical error can be estimated as:

$$d_{RE} = \frac{e_{21}}{r^{p_{RE}} - 1} \tag{4}$$

where the order of accuracy, p_{RE}, is given by:

$$p_{RE} = \frac{\ln(e_{32}/e_{21})}{\ln(r)} \tag{5}$$

$\varepsilon_{32}=S_3-S_2$, $\varepsilon_{21}=S_2-S_1$ and r is the grid refinement ratio, which in our case is $\sqrt{2}$. In the factor of safety method, a measure for the distance from the asymptotic range is given by P, which is defined as the ratio between the numerical and the theoretical order of accuracy, $P = p_{RE}/p_{th}$; when solutions are in the asymptotic range, $P\approx 1$ and the actual order of accuracy is close to the theoretical value ($p_{th}=2$). With this method, the numerical uncertainty, U_{SN}, in the last column of Table 5, is estimated through:

$$U_{SN} = \begin{cases} (2.45 - 0.85P)\,|\delta_{RE}| & 0 < P \le 1 \\ (16.4P - 14.8)\,|\delta_{RE}| & P > 1 \end{cases} \quad (6)$$

The verification studies for C_T, sinkage and trim show that, for each variable, iterative uncertainty, U_I, is acceptably small compared to grid uncertainty, U_G; consequently, the grid quality makes the major contribution to the numerical uncertainty, U_{SN}. Monotonic and oscillatory convergence is achieved for all variables ($0<R<1$) in the finer grid triplet (G1, G2, G3); on the contrary, monotonic divergence is observed in the coarser grid triplet (G2, G3, G4). Therefore, the finer grid triplet (G1, G2, G3) is used for validation study. For this case, Table 5 shows that the order of convergence for C_T is close to $P\approx0.5$, and first order accuracy is attained; for sinkage, $P\approx1.5$, which indicates a third order accuracy; finally, for trim a first order convergence is attained (a value around $P=0.5$ is found). The numerical uncertainties are very low for resistance coefficient and for sinkage, the highest value estimated is around 20% for trim angle.

Table 6 summarizes the results of the validation study. The comparison error is computed as:

$$E = \frac{S_1 - D}{D}\% \quad (7)$$

where D is the experimental data; the validation uncertainty, U_V, which takes into account both U_{SN} and experimental uncertainty U_D, is defined as:

$$U_V^2 = U_{SN}^2 + U_D^2 \quad (8)$$

When $|E|<U_V$, the combination of all the errors in D and S is smaller than U_V and validation is achieved at the U_V interval. The highest error is observed for pressure resistance coefficient and amounts to 14%. For each variable, the comparison error is lower than the corresponding U_V, indicating thus that validation is achieved at 5, 2 and 20%D for resistance, sinkage and trim, respectively. The validation level for trim is, however, large and reduction in U_V requires reduction in numerical uncertainty.

Figure 4 shows the comparison between numerical results and experimental data over the whole *Fr* range, for the catamaran configuration corresponding to *s=0.23*. Overall, a good agreement between the numerical solution and the experiments is achieved. The average comparison errors over all *Fr* amount to E=5, 9 and 4.7%D for C_T, sinkage and trim, respectively, where the highest error computed for sinkage is mainly due to the differences at larger *Fr*. The differences between C_f and the ITTC model correlation line, and between C_p and C_r equally contribute to the difference between computed and experimental C_T.

4.2 Verification and Validation for Wave Elevation

A further validation test of the numerical results is provided by comparison of the numerical wave cuts with the measurements obtained by INSEAN. Quantitative V&V is conducted for *s=0.23* and *Fr*=0.5.

The Verification and Validation procedure for point variables follows the approach presented in Wilson *et al.* (2001). The convergence ratio, R, and the order of accuracy, p, for point variables, are defined through the separate L2 norms of ε_{21} and ε_{32} according to the following formulations:

$$\langle R \rangle = \|\varepsilon_{21}\|_2 / \|\varepsilon_{32}\|_2 \qquad (9)$$

$$\langle p \rangle = \frac{\ln\left(\|e_{32}\|_2 / \|e_{21}\|_2\right)}{\ln\left(r_G\right)} \tag{10}$$

where $\langle\ \rangle$ and $\|\ \|_2$ are used to denote a profile-averaged quantity and L2 norm, respectively. Numerical errors and grid uncertainties distributions are estimated through equations (4) and (6), respectively, where p_{RE} is given by (10). The L2 norms of these distributions are, then, used to assess verification levels. In order to judge whether validation is globally achieved, the L2 norm of E and U_V distributions, obtained through Equations (7) and (8) respectively, are finally evaluated.

Figures 5a and 6a show the longitudinal wave cuts at distances *Y/b=0.125* and *Y/b=0.4166* from the hull inner side, respectively (Probes 9 and 11). It can be observed that there is a good agreement among numerical and experimental wave profiles. The verification and validation results are summarized in Table 7. The values are normalized with the maximum value of wave profile, ζ_{max}. In both cases, monotonic convergence is achieved; furthermore, results are validated at a level of 16.7% and 11.7% for Probe 9 and Probe 11, respectively. The V&V procedure shows that, overall, in order to reduce the validation uncertainty, numerical improvements related to grid quality are needed. Nonetheless, the numerical results can be advantageously used for the analysis of the flow physics involved in the interference phenomena. Distributions of E and U_V as a function of x/L_{PP} are plotted in Figures 5b and 6b.

4.3 Resistance, sinkage and trim

The results presented in this section are obtained by the use of grid G2, which is the best compromise between grid quality, computational effort and solution accuracy. The study, summarized in Table 8, shows that the solution changes for the finest grids are less than 1.2%S_1 for resistance, less than 0.3%S_1 for sinkage, and less than about 4%S_1

for trim, owing to the different order of convergence of each variable. In conclusion, even though the solutions are far from the asymptotic range, the differences between the coarser and the finer grids are relatively small, and justify, therefore, the use of the results obtained with grid G2 for the discussion of the numerical findings.

Numerical results both for the mono-hull and the catamaran, at several separation distances, are plotted in Fig.7, including C_T, C_p, C_f, sinkage and trim. About the resistance coefficient (Fig.7a), similarly to EFD data, at low and high speed, i.e. $Fr \leq 0.35$ and $Fr \geq 0.75$, the differences between the mono-hull and the catamaran are small; also, at $Fr \leq 0.45$ and $Fr \geq 0.65$, the hull configuration seems to have little influence on C_T. On the contrary, a clear dependency of C_T on the separation length, s, is observed near the hump ($Fr \approx 0.5$): as the separation distance decreases, the maximum value of C_T increases and occurs at higher Fr values. Figure 7b shows that the augmented resistance experienced by the catamaran is mostly due to an increase in the wave resistance, C_p, and consequently to the interference phenomena between the two hulls. Another hump around $Fr=0.3$ is found in the experiments, as reported in Fig.2 (Broglia *et al.*, 2014). However, the hump is not distinct in CFD simulations. A local minimum is, finally, observed in the experiments at $Fr=0.35$(Fig.2), where C_T decreases as the distance between the hull increases. Negligible or slightly favorable interference is obtained around this point. This local minimum is not predicted in CFD simulations.

Sinkage difference among all the configurations is noticeable in the whole Fr range (Fig. 7c), even for low or high Froude number values, where the resistance difference among the configurations is very small. Sinkage reaches a minimum value for $Fr=0.5$ in mono-hull, and for $Fr=0.45$ in catamaran configurations. Sinkage in catamarans is more sensitive to Fr change than mono-hull. Finally, the decrease of separation distance increases the sinkage magnitude.

Trim is negligible up to $Fr=0.35$ for all the configurations (Fig.7d). Similarly to Insel *et al.* (1992) and Molland *et al.* (1996) results, trim difference becomes clearer when

$Fr \geq 0.4$ and catamarans display significant higher trim than mono-hull. When the separation distance increases, trim angle approaches the mono-hull value. Large difference between mono-hull and catamaran can be seen in the Fr range 0.5 to 0.7, where trim reaches a maximum. At higher speed values ($Fr>0.7$), the effects of demi-hull separation distance on trim are negligible except for the $s=0.17$ case, which shows a slight difference with respect to the other configurations.

4.4 Interference

Figure 8 shows the comparison between predicted and experimental IF and C_p/C_f values vs. Fr, for all the catamaran configurations. The numerical values used in this section refer to grid G2. The agreement between experiments and computed results is satisfactory. The average errors over the whole speed range amount to 6.4%, 6.2% and 8.4% for $s=0.17$, 023 and 0.30, respectively.

At low speed (Fig.8a), i.e. $Fr \leq 0.35$, and at supercritical speed ($Fr \geq 0.75$), the IF value is close to zero. In this case, in fact, the C_T curves (Fig.7a), for all the s values, collapse on the mono-hull line and the separation distance does not have any influence on catamaran resistance, which is consistent with previous studies (Souto-Iglesias *et al.*, 2007). However, differently from Souto-Iglesias *et al.* (2007) and from Broglia *et al.* (2014), in our computations negative IF values are not observed at Fr values near 0.35. As Fr increases, $0.35<Fr\leq 0.45$, interference becomes large, owing to the larger differences between mono-hull and catamaran C_T values, but with small influence of the separation distance. The interference coefficient reaches a peak around $Fr=0.5$, similarly to the resistance coefficient behavior, and it is higher for narrower than for wider separation distance. For higher speed ($Fr>0.5$), IF reduces substantially.

Figure 8b shows C_p/C_f versus Fr. The C_p/C_f ratio directly correlates with the interference factor IF, so that for the Delft catamaran the interference is largely due to

the increased pressure component C_p, which increases significantly as the separation distance decreases.

The behavior of resistance, interference factor, sinkage and trim as a function of the Froude number will be related to the flow field and wave patterns obtained by the numerical simulations in the following sections.

4.5 Wave pattern and surface pressure

Figure 9 presents the computed wave pattern and hull surface pressure distribution for the mono-hull and for all the three catamaran configurations, at *Fr=0.3, 0.5, 0.75*.

Overall, the mono-hull displays a typical Kelvin wave pattern of diverging and transverse waves with crest at the bow. At Fr=0.5, $\lambda/L_{PP}\approx 2$ and the first trough is at the stern; as a consequence, the pressure drag is maximum. The wave patterns for the catamarans are more complex than those for the mono-hull. Strong interference phenomena are observed in the inner region, where the interacting wave systems between the hulls result in larger wave amplitudes (higher wave crests and deeper wave troughs). These are more prominent as the separation distance decreases. On the contrary, the external wave pattern is slightly affected by the presence of the twin hull.

The variation of the resistance coefficient as well as the interference factor as functions of speed and separation distance (Figures 7 and 8), are strictly related to the position and magnitude of the waves crests and troughs which develop in the inner region between demi-hulls. For a fixed separation distance, at low Fr (*Fr=0.3*), the crests and troughs are relatively small and low C_T values occur; the whole wave pattern is quite similar to the mono-hull and, as the interaction between the waves systems in the inner region is weak, the effects of separation distance on IF are negligible ($IF\approx 0$). As Fr increases, (*Fr=0.5*), the wave trough is deeper and moves downstream closer to the

stern; therefore, the resistance reaches its maximum; furthermore, due to the higher amplitude of the interfering waves with respect to the mono-hull, *IF* increases significantly. At *Fr=0.75*, the wave trough moves behind the stern and a reduction of C_T occurs; the interaction occurs downstream and a consequent reduction of *IF* is observed.

In the range of speed values where significant dependency of C_T on the separation length is observed (*Fr*≈0.5), as the gap between the hulls increases, the wave trough moves behind the stern, with lower depression; consequently, a reduction of resistance coefficient is obtained. This also implies that, at small separation length, the wave trough reaches the stern at higher speeds than the larger separation gaps, and consequently the C_T peak is shifted to higher *Fr*.

Sinkage and trim are strongly affected by the pressure distributions on the hull surfaces. From Figure 9 it is clear that the wave trough, which arrives at the stern with the highest intensity (*Fr=0.5, s=0.17*), causes a large depression on hull surface. Under these conditions, sinkage and trim reach their absolute maxima (Fig.7 c and d). Figure 10 shows the wave profile on the hull surface both for monohull and catamaran configurations. At *Fr*=0.5, the wave elevation has a crest at the bow and a trough at the stern; it creates large pressure resistance as well as large sinkage and trim values, which vary with the separation length according to Figure 7. At low speed, *Fr=0.3*, the wave height is low and only a small area of the hull surface is affected by the wave trough depression. Finally, at high speed, *Fr*=0.75, the wave length is large enough to shift the wave trough downstream of the stern; the inner wave profile on the catamaran hulls is similar to the mono-hull one; therefore, the sinkage and the trim approach the mono-hull values.

4.6 Longitudinal wave cuts

INSEAN experimental wave cuts were measured at outboard locations (1-4), inboard locations (9-12) and at centerline. Figure 11 shows a comparison between the

computational and experimental wave cuts, for the inboard location 11 (on the right) and the outboard location 3 (on the left). In Fig.11, the wave cuts are obtained for *s=0.17* using grids G2, G1 and G1R, in order to evaluate the effects of grid refinement on wave elevation predictions. This study is carried out for *Fr*=0.5 and *Fr*=0.75. Overall, the simulations show fairly good agreement for all the cases. The finer grid G1 improves the wave predictions with respect to G2, and further improvements are obtained with the finest grid G1R. However, the improvements in solution accuracy do not justify the higher computational effort due to the finer grids. In fact, for *Fr=0.75*, the average error computed using grid G2 amounts to 8.02%, it reduces to 7.6% using grid G1; the error amounts to 7.31% using grid G1R. Similar values are obtained for *Fr=0.5*.

Figures 12 to 14 show the numerical longitudinal waves elevations with varying the separation distance, in the outer side, in the inner side and at the center-plane, for several speed values. It can be observed that the external wave cuts are weakly affected by the demi-hull separation distance; in particular, along the hull (*0<X<1*) the differences between the wave cuts are negligible, while, owing to the waves interactions at and after the stern, some differences can be observed for *X>1*. However, the most relevant effects of interference occur in the inner region, where large differences occur between the inner wave profiles, with varying the separation length. The figures put in evidence the position and the magnitude of the wave trough and confirm what already observed: the wave trough becomes deeper and moves downstream with increasing ship speed, while, at fixed *Fr*, it is deeper with reducing the separation length.

4.7 Study of Reynolds number effects

The effects of Reynolds number (*Re*) on resistance, sinkage, trim and on the interference factor are studied for *s*=0.23, *Fr*=0.5 and *Re*= 2.53×10^6, 7.14×10^6, and 20.2×10^6 corresponding to L_{PP}=1.5, 3 and 6, respectively. Simulations are conducted

using grid G2a, in which the near wall distance is reduced with respect to grid G2, so that y^+ ranges from *0.1* to *0.6*.

Results are summarized in Table 9 for both *s=0.23* and the mono-hull. They show that, overall, the total resistance decreases by about 20% over the whole *Re* range, both for *s=0.23* and for the mono-hull, mainly owing to the reduction of frictional resistance component, C_f, rather than the pressure component, C_p (it decreases by less than 1% over the *Re* range).

A reduction in sinkage and trim is also registered over the whole *Re* range. Both for *s=0.23* and the mono-hull, it amounts to less than 1% and can then be neglected.

Finally, in order to evaluate the effects of *Re* on the interference coefficient, the frictional and pressure *IF* are computed within the *Re* range and the results display an increase amounting to 4.7% for frictional *IF* and a reduction by 1.3% for the pressure *IF*. Overall, the global *IF* reduces for increasing *Re*. However, the *Re* effects are small and can be, therefore, neglected.

5. CONCLUSIONS

A numerical study has been presented with focus on the effects of Froude number and of the separations distance of the hulls on the resistance, sinkage and trim of a multi-hull vessel. The aim of this work was to assess the predictive current URANS capability for a high-speed catamaran, including sinkage and trim. Consequently, a verification and validation study was carried out both for global and local variables.

The following conclusions can be drawn:

- Ship motions are predicted with reasonable accuracy for most of the cases under investigation, the maximum average error, over the whole *Fr* range, amounting to *8.9%D* for sinkage.
- The verification and validation study proves that the major source of errors is due to grid quality. Numerical errors are, however, acceptably small. Overall,

the numerical model is validated and the numerical analysis constitutes a useful tool to gain a deep insight into the flow physics involved in the interference phenomena.

- The effects of the Reynolds number, and therefore of viscosity, on interference are small compared to waves interaction and can be therefore neglected.

ACKNOWLEDGEMENTS

This work was supported by Office of Naval Research (ONR), grant of N000141010017, under the administration of Dr. Patrick Purtell. The authors appreciate INSEAN who provides the EFD data for this study.

REFERENCES

Aubault, A., Yeung, R. (2009) "Multi-hull interference wave-resistance in finite depth", Proceedings of the 24th International Workshop on Water Waves and Floating Bodies, Zelenogorsk, Russia.

Bouscasse, B., Broglia, R. and Stern, F. (2013) "Experimental investigation of a fast catamaran in head waves", Ocean Engineering, 72, pp. 318-330.

Broglia, R., Jacob, B., Zaghi, S., Stern, F. and Olivieri, A. (2014) "Experimental investigation of interference effects for high-speed catamaran", Ocean Engineering, 76, pp. 75-85.

Broglia, R., Aloisio, G., Falchi, M., Grizzi, S., Zaghi, S., Felli, M., Miozzi, M., Pereira, F., Di Felice, F., Stern, F. (2012) "Measurements of the velocity field around the DELFT 372 catamaran in steady drift", Proceedings of the 29th Symposium on Naval Hydrodynamics Gothenburg. Sweden, 26–31 August 2012.

Broglia, R., Bouscasse, B., Jacob, B., Zaghi, S., Olivieri, A. and Stern, F. (2011a) "Calm water and seakeeping investigation for a fast catamaran", Proceedings of the 11th International Conference on Fast Sea Transportation (FAST2011), Honolulu, Hawaii.

Broglia, R., Zaghi, S. and Mascio, A.D. (2011b) "Numerical simulation of interference effects for a high-speed catamaran", Journal of Marine Science and Technology, 16, pp. 254-269.

Bruzzone, D., Ferrando, M. (1995) "Numerical evaluation of the steady free surface flow for catamaran hull forms", Proceedings of the III Symposium on High Speed Marine Vehicles, Naples, 6–7 April, pp. 187–198.

Carrica, P., Hosseini, H., and Stern, F. (2012) "CFD analysis of broaching for a model surface combatant with explicit simulation of moving rudders and rotating propellers", Computers & Fluids, 53, pp. 117-132.

Carrica, P., Wilson, R.V., Noack, R.W. and Stern, F. (2007) "Ship motions using single-phase level set with dynamic overset grids", Computers & Fluids, 36, pp. 1415-1433.

Castiglione, T., Stern, F., Kandasamy, M. and Bova, S. (2011) "Numerical investigation of the seakeeping behavior of a catamaran advancing in regular head waves", Ocean Engineering 38, pp. 1806-1822.

Castiglione, T., He, W., Stern, F. and Bova, S. (2013) "URANS simulation of catamaran interference in shallow water", Journal of Marine Science and Technology; DOI 10.1007/s00773-013-0230-5.

Chen, X., Diez, M., Kandasamy, M., Campana, E.F., Stern, F. (2013) " Design optimization of the waterjet-propelled DELFT catamaran in calm water using URANS, design of experiments, metamodels and swarm intelligence", Proceedings of the 12th International Conference on Fast Sea Transportation (FAST2013), Amsterdam, Netherlands.

Cheng, X.N., Sharma, S.D., Stuntz, N. (2003) "Wave reduction by S-catamaran at supercritical speeds", J Ship Res 47, pp. 145–154.

Diez, M., He, W., Campana, E. and Stern, F. (2013a) "Uncertainty quantification of DELFT catamaran resistance, sinkage and trim for variable Froude number and geometry using metamodels, quadrature and Karhunen-Loeve expansion", Journal of Marine Science and Technology, *in press.*

Diez, M., Chen, X., Campana, E.F., Stern, F. (2013b) "Reliability-based robust design optimization for ships in real ocean environment", Proceedings of the 12th International Conference on Fast Sea Transportation (FAST2013), Amsterdam, Netherlands.

Insel, M. and Molland, A. F. (1992) "An investigation into the resistance components of high speed displacement catamarans", The Royal Institution of Naval Architects 134, pp.1–20.

Kandasamy,M., Peri, D., Ooi, S. K., Carrica, P., Stern, F., Campana, E. F., Osborne, F., Cote, J., Macdonald, N. and Waal, N. D. (2011a) "Multi-fidelity optimization of a high-speed foil-assisted semi-planing catamaran for low wake", Journal of Marine Science and Technology, 16, pp. 143-156

Kandasamy, M., He, W., Takai, T., Tahara, Y., Peri, D., Campana, E., Wilson, W. and Stern, F. (2011b) "Optimization of waterjet propelled high speed ships – JHSS and Delft catamaran", Proceedings of the 11th International Conference on Fast Sea Transportation (FAST2011), Honolulu, Hawaii.

Menter, F. R. (1994) "Two-equation eddy viscosity turbulence models for engineering applications", AIAA Journal 32, pp. 1598–605.

Milanov, E. and Zlatev, Z. (2011) "Experimental and computational studies of high-speed catamaran calm water maneuvering", RTO/AVT-161 Final Report, Chapter 24.

Millward, A. (1992) "The effect of hull separation and restricted water depth on catamaran resistance", Transactions of Royal Institution of Naval Architects 134, pp. 341–349.

Molland, A., Wilson, P., Taunton, D., Chandraprabha, S., Ghani, P. (2004) “Resistance and wash measurements on a series of high speed displacement monohull and catamaran forms in shallow water”, International Journal of Maritime Engineer, 146, pp. 19–38.

Molland A. F., Wellicome J. F. and Couser P. R. (1996) “Resistance experiments on a systematic series of high speed displacement catamarans forms: variation of length-displacement ratio and breadth-draught ratio”, Transactions of the Royal Institution of Naval Architects, 138, pp. 59-71.

Moraes, H.B., Vasconcellos, J.M., Latorre, R.G. (2004). “Wave resistance for high-speed catamaran”, Ocean Engineering, 31, pp. 2253-2282.

Noack, R. (2005). “SUGGAR: a general capability for moving body overset grid assembly”, AIAA paper 2005-5117, 17th AIAA Computational Fluid Dynamics Conference, Ontario, Canada.

Souto-Iglesias, A. R., Zamora-Rodríguez R, D. Fernández-Gutiérrez and Pérez-Rojas, L. (2007) “Analysis of the wave system of a catamaran for CFD validation”, Exp. Fluids 42, pp. 321–332.

Stern, F., Carrica, P., Kandasamy, M., Gorski, J., ODea, J., Hughes, M., Miller, R., Hendrix, D., Kring, D., Milewski, W., Hoffman, R., and Cary, C. (2006a) “Computational hydrodynamic tools for high-speed transports”, Transaction SNAME, Vol. 114.

Stern, F., Wilson, R. and Shao, J. (2006b) “Quantitative Approach to V&V of CFD simulations and certification of CFD Codes”, Int. J. Numer. Meth. Fluids 50, pp.1335–1355

Stern, F., Carrica, P. M., and Kandasamy, M. et al. (2008) “Computational hydrodynamic tools for high-speed sealift: phase ii final report”, IIHR Technical Report No. 465.

Tarafder, M.S. and Suzuki, K. (2007) “Computation of wave-making resistance of a catamaran in deep water using a potential-based panel method”, Ocean Engineering, 34, pp 1892-1900.

Van't Veer, R. (1998 a) “Experimental results of motions, hydrodynamic coefficients and wave loads on the 372 catamaran model”, TU Delft Report, No.1129.

Van′tVeer, R. (1998b) “Experimental results of motions and structural loads on the 372 catamaran model in head and oblique waves”, TU Delft Report, N.1130.

Visonneau, M., Deng, G.B., Queutey, P., Wakers, J., Mallol, B. (2012) “Anisotropic grid adaption for RANS simulation of a fast manoeuvring catamaran”, 4th High Performance Yacht Design Conference, Auckland, pp. 172-180.

Wilson, R., Stern, F., Coleman, H.W., Paterson, E.G. (2001) “comprehensive approach to verification and validation of cfd simulations- part 2: application for RANS simulation of a cargo/container ship”, Journal of Fluids Engineering, 123, pp. 803-810.

Xing, T. and Stern, F. (2010) “Factors of safety for Richardson extrapolation”, Journal of Fluids Engineering, 132, pp. 1-13.

Yeung, R.W., Wan, H. (2008) “Multihull and surface-effect ship configuration design: a framework for powering minimization”, Journal of Offshore Mechanics and Arctic Engineering, 130, pp. 1-9.

Zaghi, S., Broglia, R., Di Mascio, A. (2011) “Analysis of the interference effects for high-speed catamarans by model tests and numerical simulations”, Ocean Engineering, 38 (17–18), 2110–2122.

Zlatev, Z., Milanov, E., Chotukova, V., Sakamoto, N., Stern, F. (2009) “Combined model-scale EFD-CFD investigation of the maneuvering characteristics of a high speed catamaran”, 10th International Conference on Fast Sea Transportation FAST 2009, Athens, Greece.

Table captions

Table 1 Main particulars of Delft catamaran model.

Table 2 Boundary conditions.

Table 3 Grids designed for catamaran studies.

Table 4 Grids and simulation conditions for the different studies.

Table 5 Verification for *s=0.23* at *Fr=0.5*.

Table 6 Validation for s=0.23 at Fr=0.5 for grid triplet G1, G2, G3.

Table 7 Verification and validation for wave profiles (*s*=0.23, *Fr*=0.5).

Table 8 CFD simulations with different grids.

Table 9 Effects of Reynolds number on resistance, sinkage and trim for catamaran configuration *s*=0.23 and mono-hull, at *Fr*=0.5.

Table 1. Main particulars of Delft catamaran model.

Main Particulars		Symbol	Unit	BSHC	TU Delft	INSEAN	CFD
Length between perpendiculars*		L_{PP}	m	3.63	3.00	3.00	3.00
Depth of towing tank		h		0.41	0.87	2.17	0.70
Beam overall		B		0.31			
Beam demihull		b		0.08			
Distance between center of hulls		s		0.23			
Draft		T		0.05			
Form factor		k		0			
Longitudinal center of gravity		LCG		0.53	0.53		
Vertical center of gravity		KG		0.04	0.06		
Tow Point		L_T		†	0.53		
		h_T			0.06		
Depth/ Draft		h/T		8.2	17.3	43.3	14.0
Temperature		C	$°C$	10.4	20.0	20.1	15.0
Fr range	C_T , sinkage and trim	Fr		0.17-0.64	0.18-0.75	0.10-0.80	0.30-0.80
	Wave cuts				0.3, 0.5, 0.75	0.3, 0.5, 0.75	0.3, 0.5, 0.75
Re (at Fr=0.5)		Re	10^6	9.05	8.13	8.12	7.14
Facility Bias	C_T	U_{FB} Δ		3.11	3.07	4.10	
	C_r			3.14	2.63	2.93	
	Sinkage			12.77	10.13	4.98	
	Trim			3.91	2.80	5.59	

* Note: L is dimensional; other length parameters are non-dimensionalized by L

† Note: BSHC uses PMM with 2 contact points on the model

Δ Note: U_{FB} is %Max($D^i_{Avg.}$)

Table 2. Boundary conditions.

Description	ϕ	p	k	ω	U	V	W
Inlet (X=-0.4)	$f = -z$	$\frac{\partial p}{\partial n} = 0$	$\frac{9.0x10^{-3}}{\mathrm{Re}}$	9.0	1	0	0
Exit (X=3.6)	$\frac{\partial f}{\partial n} = 0$	$\frac{\partial p}{\partial n} = 0$	$\frac{\partial k}{\partial n} = 0$	$\frac{\partial w}{\partial n} = 0$	$\frac{\partial^2 U}{\partial n^2} = 0$	$\frac{\partial^2 V}{\partial n^2} = 0$	$\frac{\partial^2 W}{\partial n^2} = 0$
Far-field (Z=-0.7)	$\frac{\partial f}{\partial n} = 1$	$\frac{\partial p}{\partial n} = 0$	$\frac{\partial k}{\partial n} = 0$	$\frac{\partial w}{\partial n} = 0$	1	0	0
Far-field (Z=0.7)	$\frac{\partial f}{\partial n} = -1$	-	$\frac{\partial k}{\partial n} = 0$	$\frac{\partial w}{\partial n} = 0$	$\frac{\partial U}{\partial n} = 0$	$\frac{\partial V}{\partial n} = 0$	$\frac{\partial W}{\partial n} = 0$
Far-field (Y=1.3)	$\frac{\partial f}{\partial n} = 0$	$\frac{\partial p}{\partial n} = 0$	$\frac{\partial k}{\partial n} = 0$	$\frac{\partial w}{\partial n} = 0$	$\frac{\partial U}{\partial n} = 0$	$\frac{\partial V}{\partial n} = 0$	$\frac{\partial W}{\partial n} = 0$
Symmetry (Y=0)	$\frac{\partial f}{\partial n} = 0$	$\frac{\partial p}{\partial n} = 0$	$\frac{\partial k}{\partial n} = 0$	$\frac{\partial w}{\partial n} = 0$	$\frac{\partial U}{\partial n} = 0$	0	$\frac{\partial W}{\partial n} = 0$
No slip (ship hull)	$\frac{\partial f}{\partial n} = 0$	-	0	$\frac{60}{\beta \mathrm{Re} \Delta y_1^2}$	0	0	0

Table 3. Grids designed for catamaran studies.

Grid	Dimensions			Total	y^+ (Fr=0.5, Re=7.1×10^6)
	Hull in and out	Background	Refinement		
G1R	244×93×139	436×196×142	601×181×181	38.1 M	0.6
G1	244×93×139	436×196×142		18.4 M	0.6
G2	172×66×98	309×139×101		6.6 M	0.9
G2a	172×66×98	309×139×101		6.6 M	0.2
G3	122×47×70	218×98×71		2.3 M	1.4
G4	86×33×49	155×70×51		0.8 M	2.3

Table 4. Grids and simulation conditions for the different studies.

Study	Grid	Simulation conditions		
		Configuration	*Fr*	*Re*(10^6)
Verification	G1, G2, G3, G4	*s*=0.23	0.5	7.14
Interference	G2	Monohull, *s*=0.17, 0.23, 0.30	0.3-0.8	4.29-11.43
Refinement	G1, G1R	*s*=0.17	0.5, 0.75	7.14, 10.72
Re	G2a	Monohull, *s*=0.23	0.5	2.53, 7.14, 20.2

Table 5. Verification for *s=0.23* at *Fr=0.5*.

Param.	Triplet	*R*	*P*	U_1% U_G	$U_{SN}=U_G$%*D*
C_T	G1,G2,G3	0.71	0.49	0.27	5.66
	G2,G3,G4	1.62	MD		
Sink	G1,G2,G3	0.37	1.43	0.43	1.41
	G2,G3,G4	-0.37	OC	3.91	1.12
Trim	G1,G2,G3	0.73	0.45	0.10	20.57
	G2,G3,G4	0.753	0.33	0.07	45.82

Table 6. Validation for *s=0.23* at *Fr=0.5* for grid triplet G1,G2,G3.

Param.	INSEAN EFD†			
	U_D	U_{SN}	U_V	*E*
C_T	0.21	5.66	5.66	- 4.92
C_f				9.05
C_p				-14.76
Sink	1.31	1.41	1.92	0.85
Trim	2.91	20.57	20.78	-1.39

†Note: U_D, U_{SN}, U_V and *E* are *%D*,

Table 7. Verification and validation for wave profiles (*s*=0.23, *Fr*=0.5).

Location	Verification			Validation		
	R_G	*P*	U_G	U_D	U_V	*E*
Probe 9	0.67	0.58	15.01	7.45	16.76	11.56
Probe 11	0.66	0.58	10.74	4.72	11.73	11.58

†Note: U_D, U_G, U_V and *E* are $\%\zeta_{max}$

Table 8. CFD simulations with different grids.

s	*Fr*	*Grid*	$C_T \times 10^3$		Sink		Trim	
			S	$\varepsilon_{12}\%S_1$	*S*	$\varepsilon_{12}\%S_1$	*S*	$\varepsilon_{12}\%S_1$
0.23	0.50	G1	7.322	1.17	-11.79	0.27	-1.74	3.71
		G2	7.236	1.66	-11.76	0.73	-1.67	5.24
		G3	7.116		-11.68		-1.58	

$\varepsilon_{12}\%S_1=(S_1-S_2)\%S_1$, where S_1 is the result of finer grid and S_2 is the coarse grid

Table 9. Effects of Reynolds number on resistance, sinkage and trim for catamaran configuration s=0.23 and mono-hull, at Fr=0.5.

s	*L (m)*	$Re(10^6)$	*E**							
			$C_f \times 10^3$	$C_p \times 10^3$	$C_T \times 10^3$	*Sinkage (mm)*	*Trim(deg)*	$C_{T,cat} - C_{T,mono}$	IF_f	IF_p
0.23	1.5	2.53	18.5	0.4	9.5	-0.5	-0.4	**1.0**	-1.7	0.7
	3.0	7.14								
	6.0	20.2	-15.4	0.02	-7.8	0.2	0.5	**-0.35**	3.0	-0.6
mono	1.5	2.53	19.2	0.1	11.5	0.3	-0.1			
	3.0	7.14								
	6.0	20.2	-15.9	0.23	-9.5	-0.1	0.1			

Note: $E^*=(S-S^*)\%S^*$, S^* is the result of L_{PP}=3.0m.

Figures captions

Figure 1. Lines plan of the Delft catamaran 372. a) Lines plan b) Side view c) 3D View.

Figure 2. Comparison of EFD from different facilities at the design separation distance s=0.23. a) Total resistance coefficient; b) Residuary resistance and friction coefficients; c) Non-dimensional sinkage; d)Non-dimensional trim.

Figure 3. Particulars of the computation domain.

Figure 4. CFD simulations (Grid G2) for catamaran s=0.23 compared with INSEAN EFD. a) Total resistance coefficient; b) Pressure and friction coefficients; c) Non-dimensional sinkage; d) Non-dimensional trim.

Figure 5. Grid study and validation of wave profile at Probe 9. The error values are normalized with the maximum height of wave profile ζ_{max}.

Figure 6. Grid study and validation of wave profile at Probe 11. The error values are normalized with the maximum height of wave profile ζ_{max}.

Figure 7. CFD simulations for mono-hull and catamaran (Grid G2). a) Total resistance coefficient b) Pressure and friction resistance coefficients; c) Non-dimensional sinkage; d) Non-dimensional trim.

Figure 8. a) Interference factor: numerical values compared with INSEAN EFD; b) Numerical $\boldsymbol{C_p/C_f}$**.**

Figure 9. Wave patterns and surface pressure distribution on the hull surface at three *Fr* for mono-hull and for catamaran at three separation distances.

Figure 10. Numerical wave profiles on the hull surface at three *Fr*, for mono-hull and catamaran, at three separation distances. Inner side on hull (*left*), outer side on hull (*right*).

Figure 11. Longitudinal wave cuts at *Fr=0.3*, *Fr=0.5* and *Fr=0.75* for the catamaran configuration s=0.17. Comparison between numerical results obtained using grids G2, G1 and G1R, and INSEAN EFD. Left: Location 3(*outboard*); Right: Location 11 (*inboard*).

Figure 12. Numerical longitudinal wave cuts at *Fr=0.3*. a) outboard location; b) inboard location 11; c) center line.

Figure 13. Numerical longitudinal wave cuts at *Fr=0.5*. a) outboard location; b) inboard location 11; c) center line.

Figure 14. Numerical longitudinal wave cuts at *Fr=0.75*. a) outboard location; b) inboard location 11; c) center line.

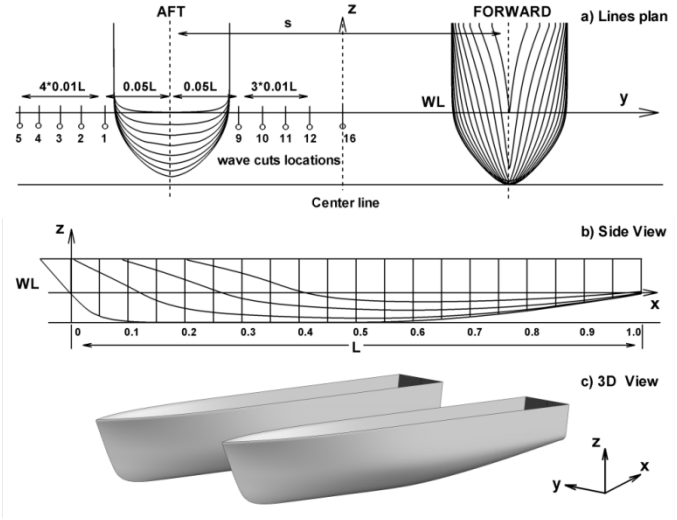


Figure 1. Lines plan of the Delft catamaran 372.
a) Lines plan b) Side view c) 3D View.

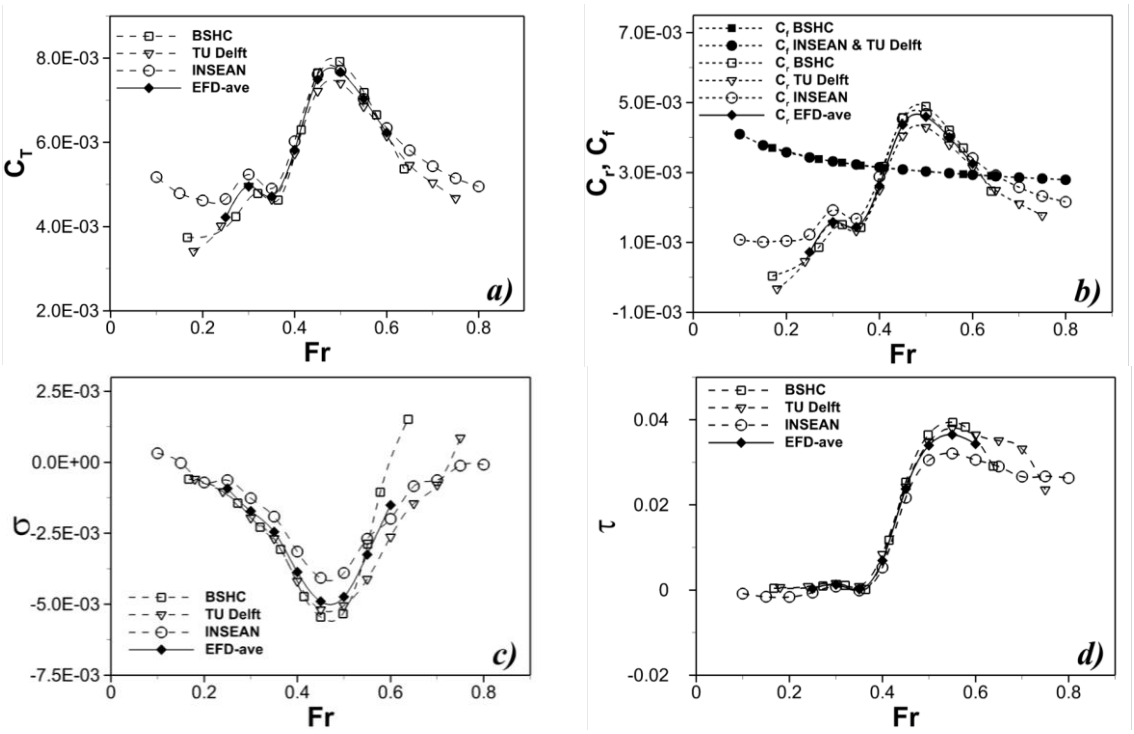


Figure 2. Comparison of EFD from different facilities at the design separation distance *s=0.23*. a) Total resistance coefficient; b) Residuary resistance and friction coefficients; c) Non-dimensional sinkage; d) Non-dimensional trim.

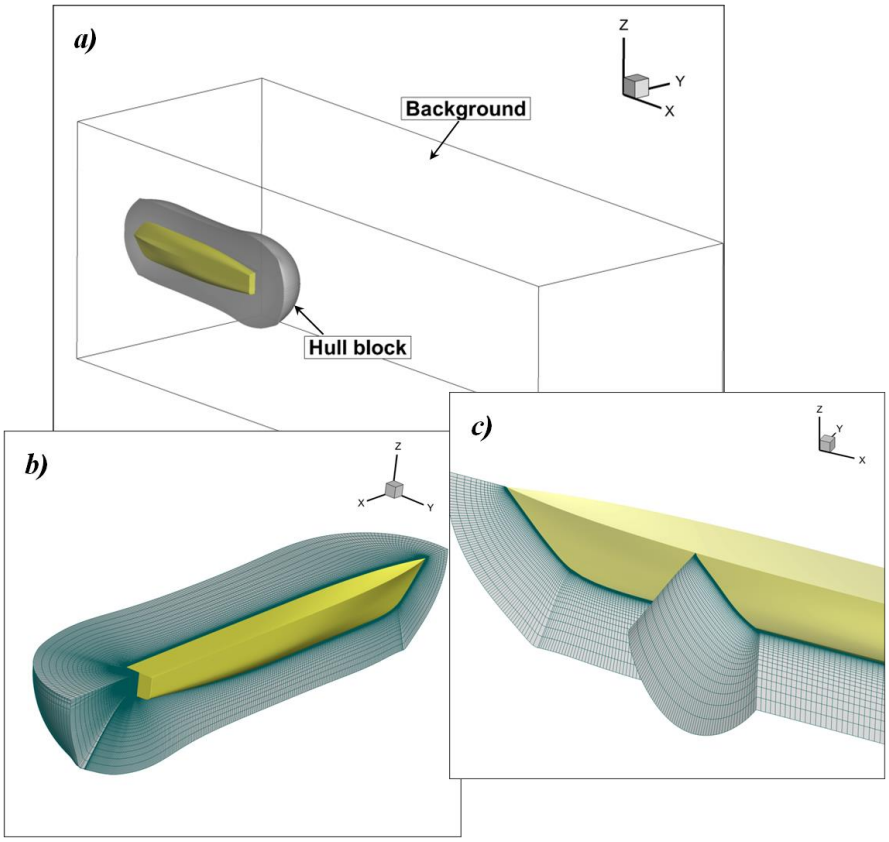


Figure 3. Particulars of the computational domain.

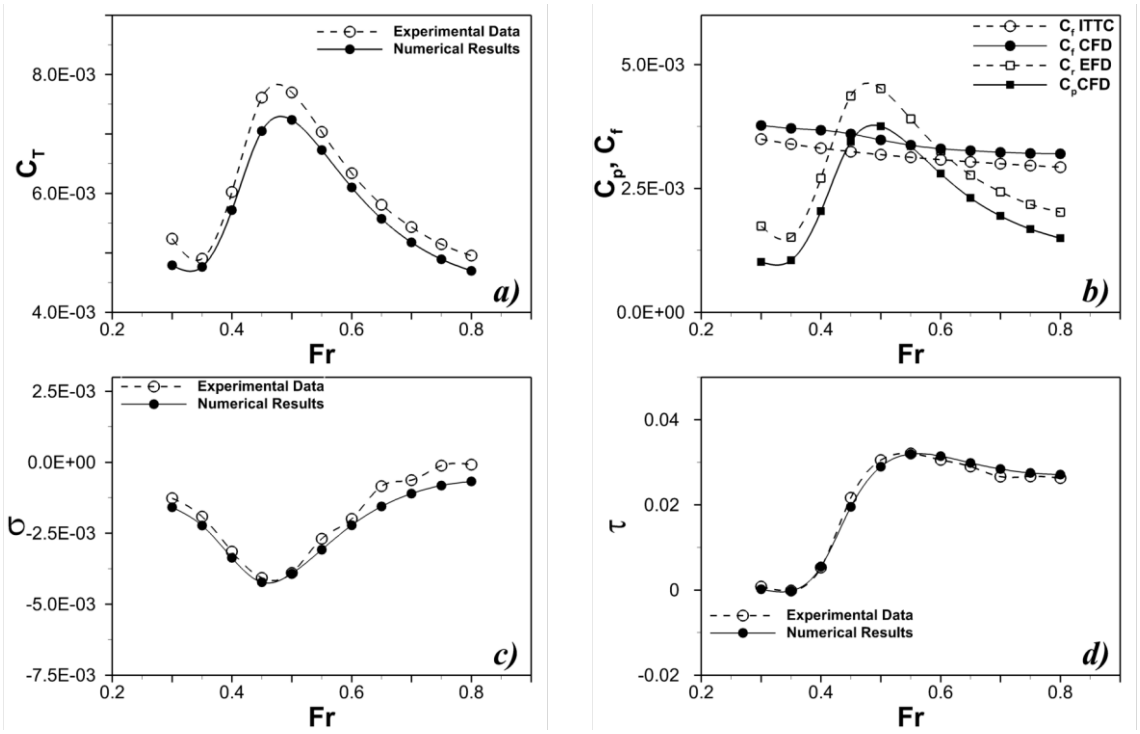


Figure 4. CFD simulations (Grid G2) for catamaran *s=0.23* compared with INSEAN EFD. a) Total resistance coefficient; b) Pressure and friction coefficients; c) Non-dimensional sinkage; d) Non-dimensional trim.

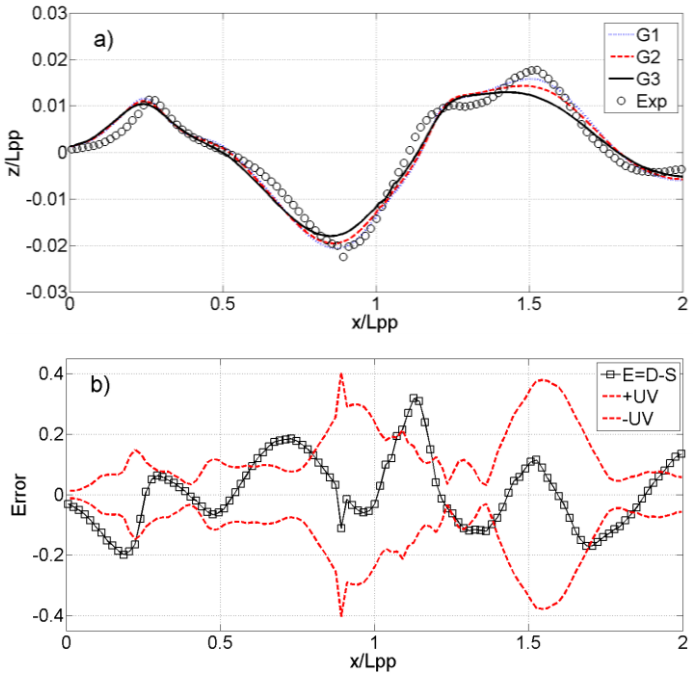


Figure 5. Grid study and validation of wave profile at Probe 9. The error values are normalized with the maximum height of wave profile ζ_{max}.

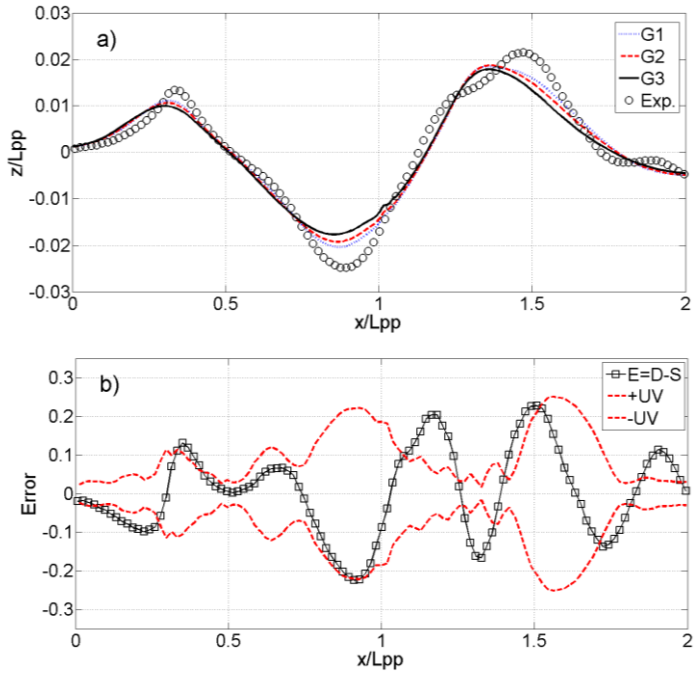


Figure 6. Grid study and validation of wave profile at Probe 11. The error values are normalized with the maximum height of wave profile ζ_{max}.

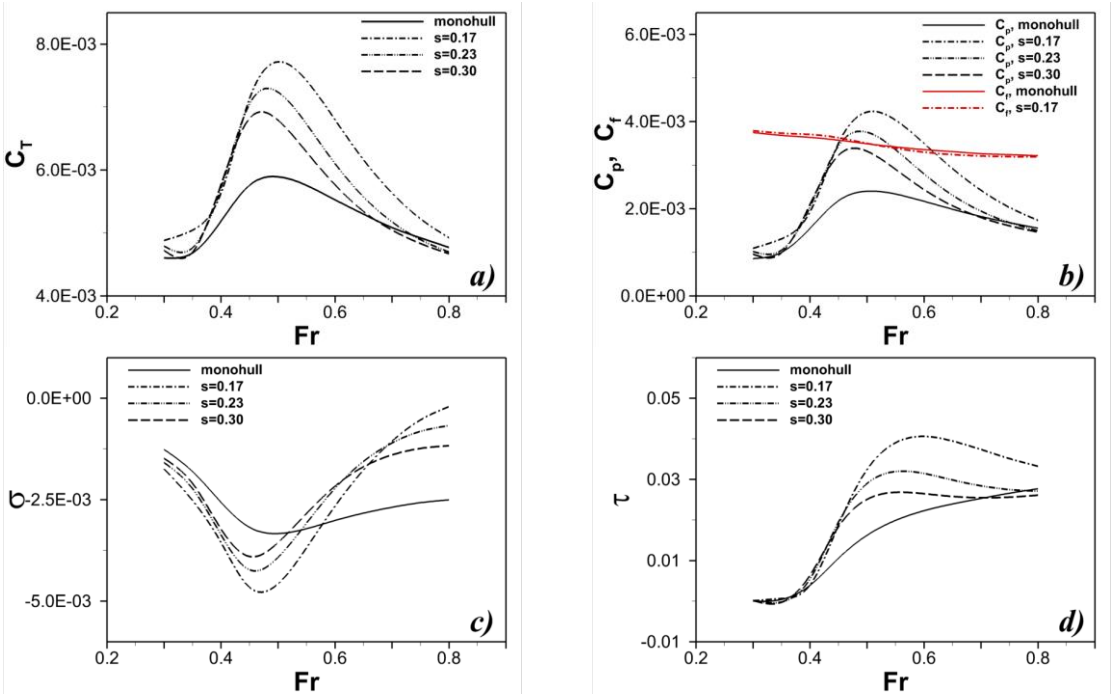


Figure 7. CFD simulations for mono-hull and catamaran (GridG2). a) Total resistance coefficient; b) Pressure and friction coefficients; c) Non-dimensional sinkage; d) Non-dimensional trim.

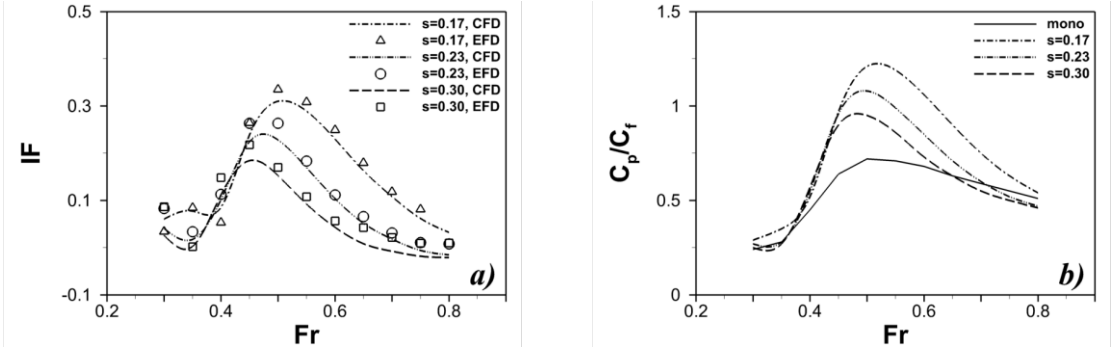


Figure 8. Analysis of *IF* (a) and C_p/C_f (b) as a function of Froude number and hull distance (CFD from grid G2, EFD form INSEAN).

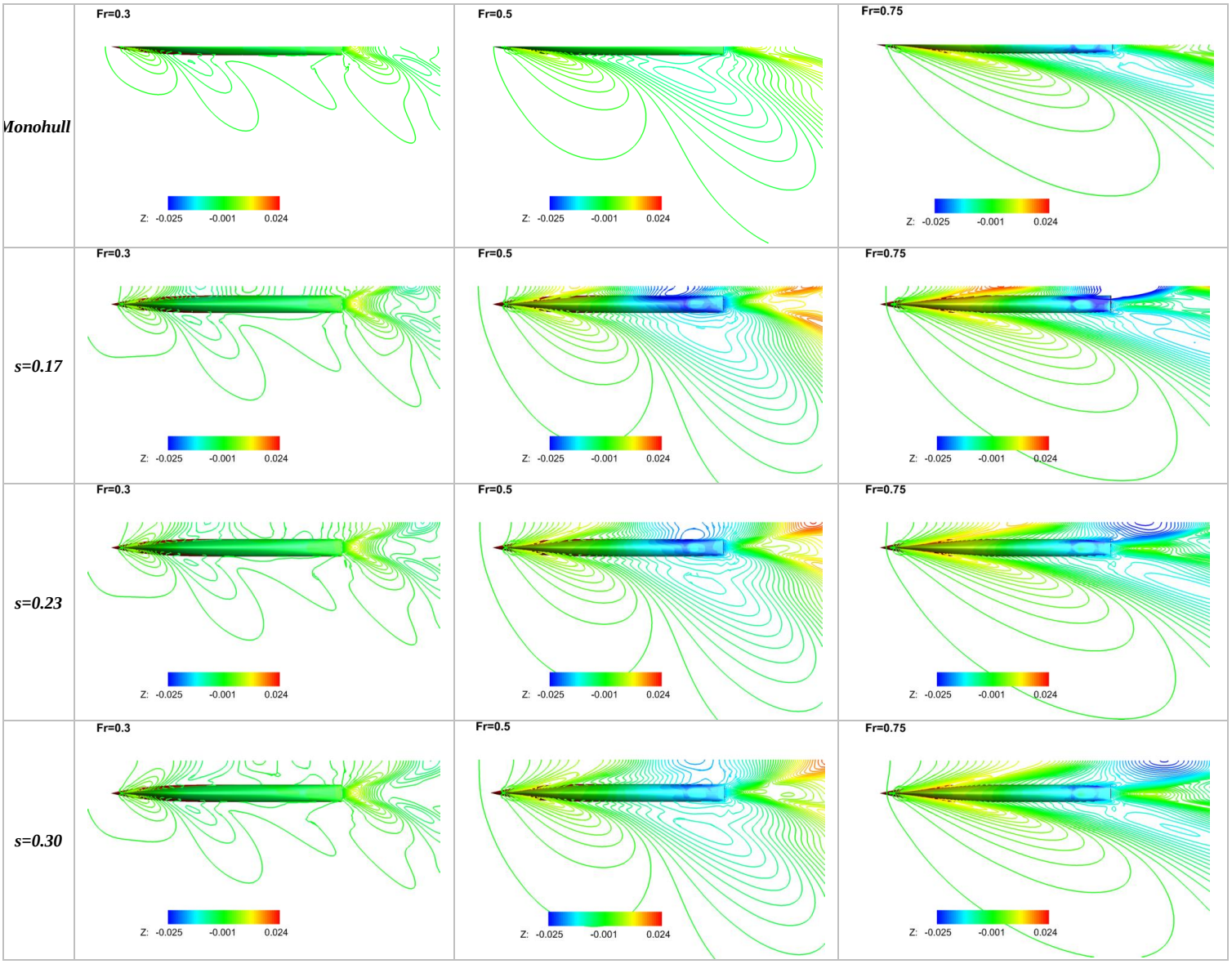


Figure 9. Wave patterns and surface pressure distribution on the hull surface at three *Fr* for mono-hull and for catamaran at three separation distances.

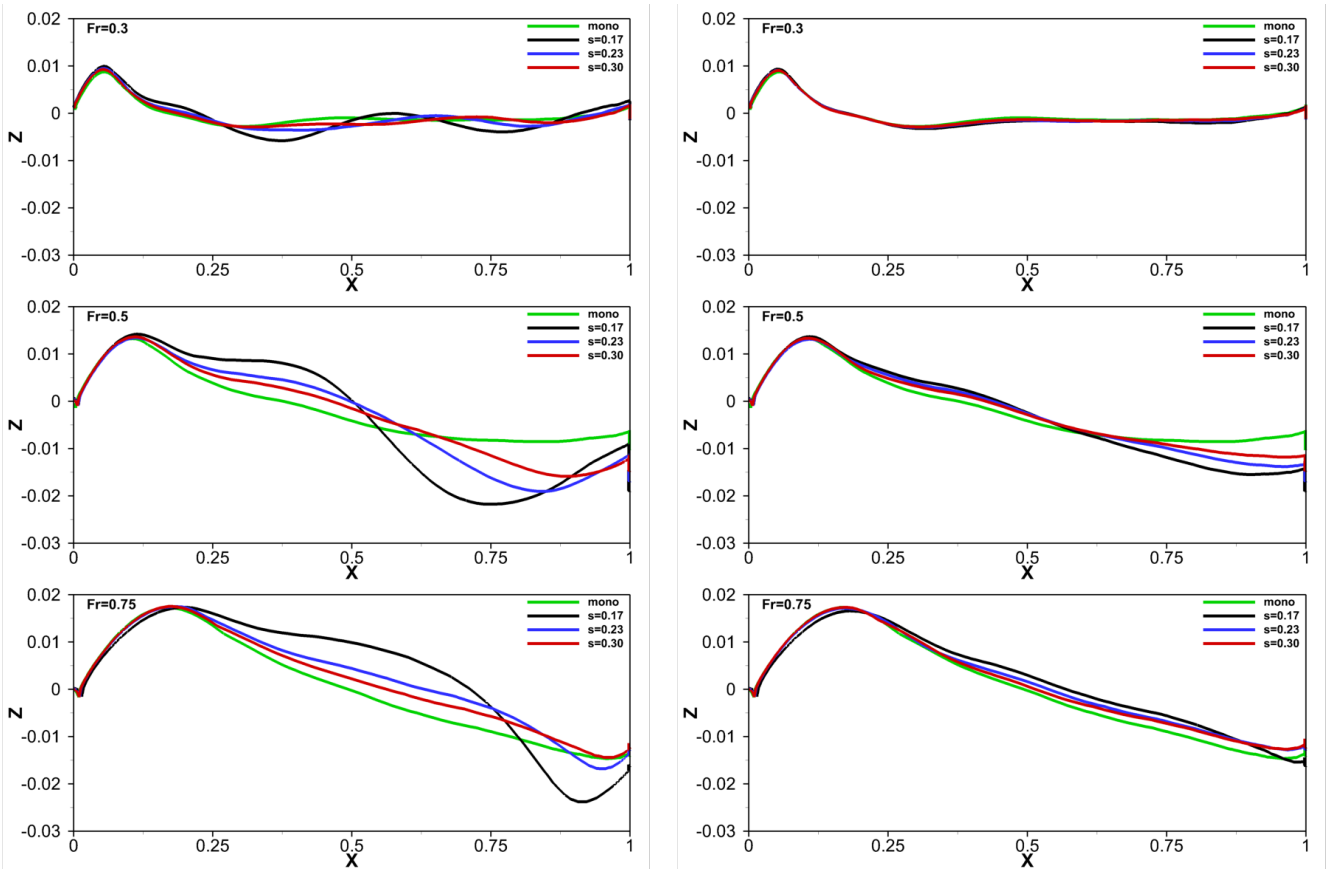


Figure 10. Numerical wave profiles on the hull surface at three *Fr*, for mono-hull and catamaran, at three separation distances. Inner side on hull *(left)*, outer side on hull *(right*)**.**

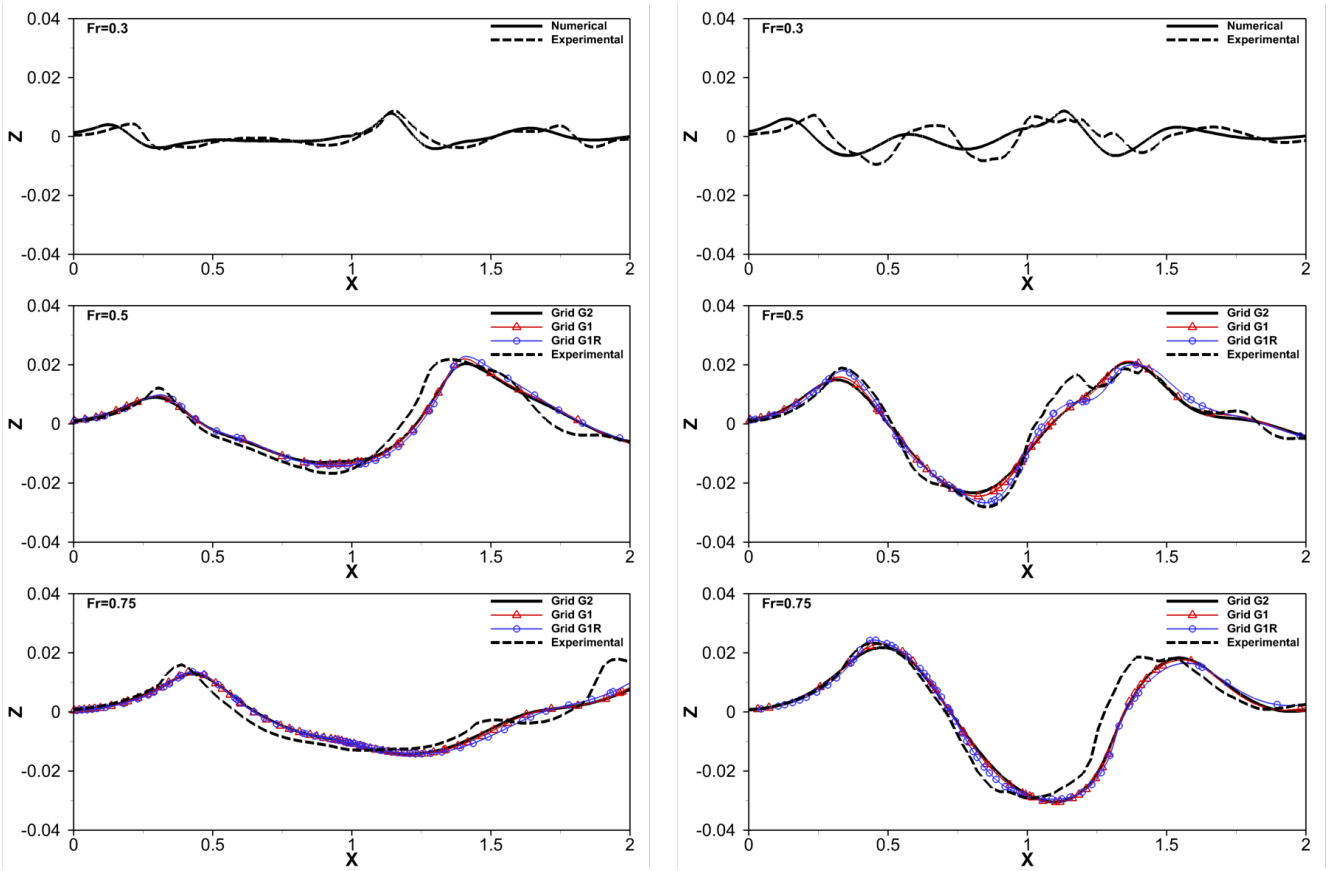


Figure 11. Longitudinal wave cuts at *Fr*=0.3, *Fr=0.5* and *Fr=0.75* for the catamaran configuration *s*=0.17. Comparison between numerical results obtained using grids G2, G1 and G1R, and INSEAN EFD. *Left:* Location 3(outboard); *Right:* Location 11 (inboard).

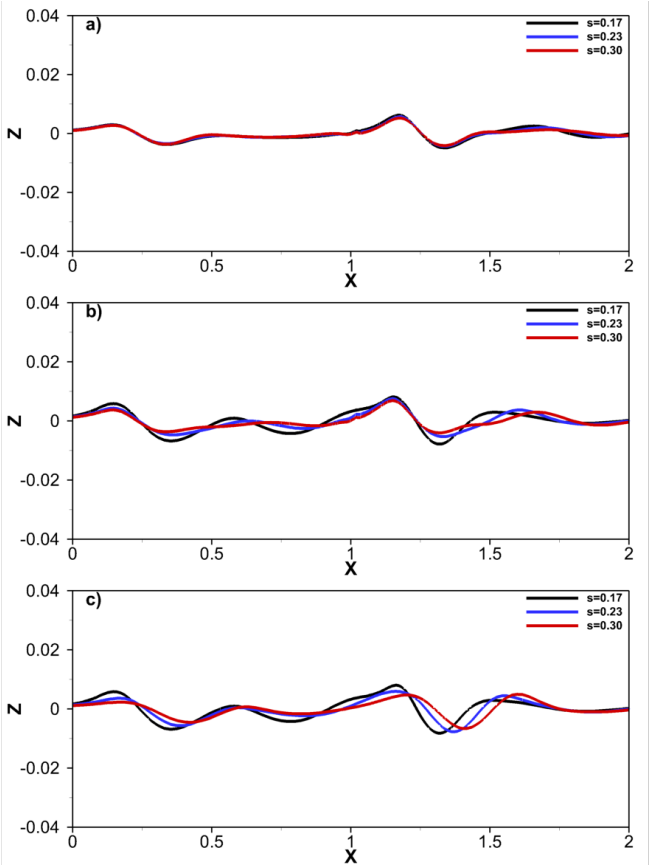


Figure 12. Numerical longitudinal wave cuts at *Fr*=0.3(Grid G2). a) outboard location; b) inboard location 11; c) center line.

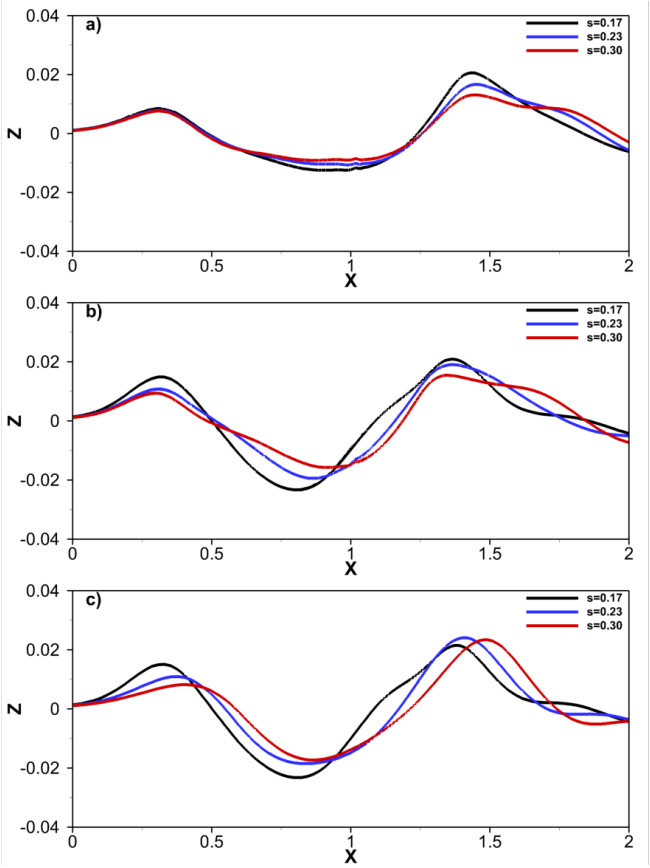


Figure 13. Numerical longitudinal wave cuts at *Fr*=0.5 (Grid G2). a) outboard location; b) inboard location 11; c) center line.

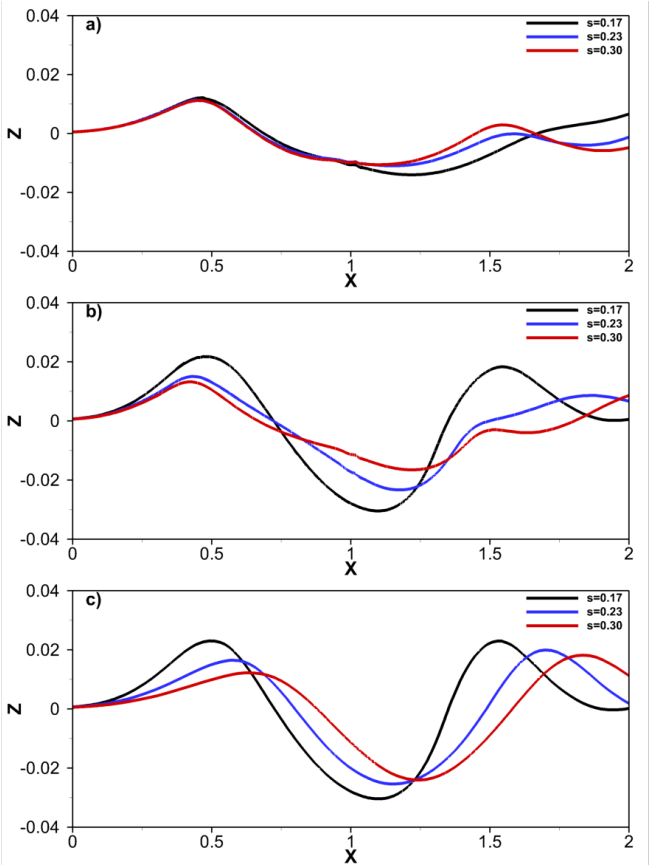


Figure 14. Numerical longitudinal wave cuts at *Fr*=0.75(Grid G2). a) outboard location; b) inboard location 11; c) center line.